Report No. DOT/FAA/NR-90/2

(2)

Project Report
ATC-172

Divergence Detection in Wind Fields Estimated by an Airport Surveillance Radar

T.A. Noyes

15 October 1990

Lincoln Laboratory

MASSACHUSETTS INSTITUTE OF TECHNOLOGY

LEXINGTON, MASSACHUSETTS

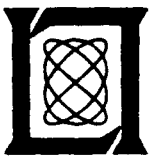

Prepared for the Federal Aviation Administration.

TECHNICAL REPORT STANDARD TITLE PAGE

1. Report No.	2. Government Accession No.	3. Recipient's Catalog No.
ATC-172	DOT/FAA/NR-90/2	

4. Title and Subtitle	5. Report Date
Divergence Detection in Wind Fields Estimated by an Airport Surveillance Radar	15 October 1990
	6. Performing Organization Code
7. Author(s)	8. Performing Organization Report No.
Terri A. Noyes	ATC-172
9. Performing Organization Name and Address	10. Work Unit No. (TRAIS)
Lincoln Laboratory, MIT P.O. Box 73 Lexington, MA 02173-9108	11. Contract or Grant No. DTFA-01-L-83-4-10579
12. Sponsoring Agency Name and Address	13. Type of Report and Period Covered
Department of Transportation Federal Aviation Administration Systems Research and Development Service Washington, DC 20591	Project Report
	14. Sponsoring Agency Code

15. Supplementary Notes

This report is based on studies performed at Lincoln Laboratory, a center for research operated by Massachusetts Institute of Technology under Air Force Contract F19628-90-C-0002.

16. Abstract

This report assesses a technique for automatic detection of hazardous divergence in velocity fields estimated by an Airport Surveillance Radar (ASR).

~~We evaluate~~ a least-squares approach to radial divergence estimation through a performance analysis based on simulated data. This approach is compared to an existing decision-based radial shear finding method used for the Terminal Doppler Weather Radar (TDWR).

Empirical results derived by the application of the two techniques to data collected at ASR testbeds in Huntsville, Alabama and in Kansas City, Missouri are presented.

Results indicate that a simple, least-squares divergence estimator combined with time association logic to increase temporal continuity of algorithm output is an equally effective means of detecting divergent wind shear in velocity fields estimated from ASR signals.

17. Key Words		18. Distribution Statement
ASR	divergence	Document is available to the public through the National Technical Information Service, Springfield, VA 22161.
microburst	algorithm	
wind shear		

19. Security Classif. (of this report)	20. Security Classif. (of this page)	21. No. of Pages	22. Price
Unclassified	Unclassified	52	

FORM DOT F 1700.7 (8-72) Reproduction of completed page authorized

ABSTRACT

This report assesses a technique for automatic detection of hazardous divergence in velocity fields estimated by an Airport Surveillance Radar (ASR).

We evaluate a least-squares approach to radial divergence estimation through a performance analysis based on simulated data. That approach is compared to an existing decision-based radial shear finding method used for the Terminal Doppler Weather Radar (TDWR).

Empirical results derived by the application of the two techniques to data collected at ASR testbeds in Huntsville, Alabama and in Kansas City, Missouri are presented.

Results indicate that a simple, least-squares divergence estimator combined with time association logic to increase temporal continuity of algorithm output is an equally effective means of detecting divergent wind shear in velocity fields estimated from ASR signals.

ACKNOWLEDGMENTS

I would like to express my sincere appreciation to the following people who contributed to this work. To Mark Weber, who provided valuable feedback and encouragement; Barbara Forman, Matthew Kahn, and Bill Moser, who developed analysis and scoring tools; Joe Cullen, who provided expert meteorological support; Jim Pieronek, Oliver Newell, Bill Drury and Bill Moser (again), who engineered the ASR-9 emulation radar and computer hardware; Wes Wilson of NCAR for feedback and encouragement; and Wes Johnston, Jay Laseman and Gene Telles (GE Government Services) who spent countless hours operating the Huntsville and Kansas City testbeds to record and log the data used in Section IV of this report.

This work is being performed under Interagency Agreement No. DTFA01-84-Z-02030 and is sponsored by the Federal Aviation Administration.

TABLE OF CONTENTS

LIST OF ILLUSTRATIONS

DIVERGENCE DETECTION IN WIND FIELDS ESTIMATED BY AN AIRPORT SURVEILLANCE RADAR

I. INTRODUCTION

This report presents a divergence-based approach to microburst hazard detection in single-Doppler radial velocity fields estimated by an Airport Surveillance Radar (ASR).

A. Background

A study based on two years of data collected at an ASR testbed in Huntsville, Alabama demonstrated the potential effectiveness of windshear detection with an ASR-9 modified to produce weather radial velocity estimates as well as reflectivity estimates.* [Weber and Noyes, 1988]. The Microburst Divergent Outflow Algorithm (MDOA) used in that study was a slightly modified version of a technique developed by Merritt [1987] for use with a Terminal Doppler Weather Radar (TDWR). Application of the TDWR technique to ASR wind estimates from Huntsville thunderstorms yielded excellent hit-miss performance statistics, meeting standards set by the FAA TDWR System Requirements Statement.

Despite good performance, the complexity of the TDWR-derived technique makes difficult both decomposition and evaluation of its individual stages and optimization of its parameter set. The research described in this report investigates replacement of the decision-based, highly nonlinear technique with a simple gradient estimator combined with a conventional image segmentation process. Furthermore, the divergence-field based algorithm (DBA) exploits the radar's rapid 4.8 second rotation rate, and is relatively insensitive to velocity estimate errors caused by the short time on target.

B. Scope

The goal of this report is to present and assess the different approach taken. To do so, the TDWR algorithm is used as a "yardstick" for performance measurements.

Section II describes the radial divergence computation employed by the new algorithm, and attempts to quantify the spatial accuracy of outputs from both algorithms at this stage using a simulated data set. Section III provides a detailed description of the remaining phases of the DBA. Empirical results obtained from the application of the algorithms to selected Huntsville (1988) and Kansas City (1989) cases are presented in Section IV. Section V then summarizes both the empirical and simulation results.

The simulation study of Section II employs a version of the MDOA adapted from TDWR in 1987.** Appendix A provides an overview of the real-time ASR MDOA algorithm, adapted from the TDWR algorithm in 1989 and used to produce the visual output and statistics for Section IV [Newell, 1990].

---

* The signal processing strategy used to produce low altitude wind velocity estimates from ASR high and low beam spectral data is described in [Weber, 1989].

** The TDWR MDOA algorithm described in Merritt [1987] has since undergone changes. Results from the revised algorithm are described in Merritt et. al. [1989].

II. INITIAL RADIAL DIVERGENCE ESTIMATION

Initial divergence detection is perhaps the most crucial of all algorithm stages because it is at that stage that the delineation of hazard area occurs or is forfeited. It may be possible to correct for spatial overestimation or false alarming at this initial stage by using grouping criterion at later stages to filter isolated noise points or regions; however, underestimation of hazard area and later abstraction away from the data level results in unrecoverable information loss.

This section presents and evaluates the crucial first phase of pointwise radial divergence detection of the divergence-based microburst detection algorithm (DBA) developed for the ASR. The algorithm was previously discussed in [Weber and Noyes, 1989].

A. Method

1. Point Shear Identification

The first step of the DBA performs a least-squares linear fit about each range gate along a velocity radial, where shear is the slope of the best fit line. The formula, which is a simplification of the general case due to the equal spacing of data points in range, may be written as

$$\text{shear}_n = \left(\sum_{i=-k,k} i \; v_{n-i} \right) / \left(\Delta r \sum_{i=-k,k} i^2 \right)$$

where k is the half-width of the fit window, v_i is the velocity at point i, and Δr is the range gate spacing.

Figure 2.1 shows the velocity field for one scan through a microburst near the ASR testbed in Huntsville, Alabama on August 15, 1988. Also shown are divergence fields resulting from the application of the least-squares operator with widths ranging from 3 gates (360 m) to 11 gates (1320 m). The color table for the divergence fields was chosen in order to display only positive shear estimates, with thresholds of 2.5, 5, and 10 x 10^{-3} m/s / m used to highlight degrees of hazard. Note the reduced noisiness and increased blurring of the features achieved as the window size for the least-squares fit increases; the shear images shown are otherwise unfiltered.

It is obvious that the least-squares or any similar computational technique will have a noise resiliency versus spatial accuracy tradeoff. A least-squares filter which is too small, while providing an accurate response to true signals, will be too sensitive to isolated noise points; one which is too large, while filtering noise, may spatially under or overestimate the hazard extent and may underestimate the hazard strength. Discussion of tradeoffs in the selection of a least-squares fit window for the algorithm is a topic of this section.

The field of divergence estimates resulting from this last stage is subjected to a minimum shear criterion by applying a site-adaptable threshold. The threshold would typically correspond to a windspeed loss of 10 m/s over 4 km, or pointwise shear of 2.5 x 10^{-3} m/s / m.

2. Temporal Filtering of Point Shear Estimates

The ASR's rapid rotation rate of 4.8 seconds makes it plausible to apply time continuity constraints to the thresholded least-squares divergence estimates. This is achieved by incre-

menting either a positive or negative map at each range gate on successive scans, depending on whether the divergence threshold was or was not exceeded. When a cell in the positive map is incremented, the corresponding cell in the negative map is zeroed. The positive map is input to the subsequent 2-D region finding operation, described in Section III. The *PT_START_THRESH* parameter indicates the value in the positive map (or the number of scans over which shear must have been seen at a point) required for it to be considered part of a shear region. Conversely, the variable *PT_END_THRESH* indicates the value in the negative map which will cause the corresponding positive map entry to be brought back to 0, thereby excluding that cell from any shear region.

A simulation was performed to quantify the effects of the time logic employed by the DBA to insure feature continuity, and results were used as a basis for selecting algorithm parameters. The parameters chosen must 1) increase by coasting the probability of detection for features which are fairly prevalent, and 2) decrease the probability of detection for features which are intermittent.

For each of 20 values corresponding to frequency of occurence sampled at 5 percent intervals between 0 percent and 1 percent, 10,000 random numbers following a uniform distribution were generated to correspond to values on 10,000 scans. To create the original x percent frequency of occurence, then, it was determined if each number generated was below or above the value x. If below x, the element was considered missing and a negative indicator was incremented; if above x, a positive value was incremented, and the algorithm time logic was applied. The graph of 2.2 shows the quantitative effect of the time smoothing logic on feature probability of detection for different combinations of *START_THRESH* and *END_THRESH* parameters. Figure 2.2 plots the original frequency of occurence against the frequency after time smoothing for the parameters shown.

The settings *PT_START_THRESH = 3, PT_END_THRESH = 2* were chosen to cause features which exist less than 40 percent of the time to be suppressed, and to increase the frequency of features occuring more than 40 percent of the time. The effectiveness of these settings was independently verified through end-to-end testing of the algorithm. The other curves are provided for comparison.

As an alternative to temporal point shear smoothing by the algorithm, we are also considering more aggressive time smoothing of the velocity estimates in the signal processor.

B. Evaluation

1. Performance Metrics

Here we evaluate the least-squares approach to radial divergence detection by application to simulated data. The simulated data set allows for control of the features of the microburst (strength, size) and the characteristics of the velocity field (estimate variance) which cannot be achieved with real data.

For the purposes of this study, radial divergence is modeled as the ascending (half period) portion of a sine wave. The sine wave model has been acknowledged as a reasonable approximation to the low-frequency components of a radial microburst profile [Elmore et. al., 1989]. Noise exhibiting a Gaussian distribution is added to simulate the statistical uncertainties in velocity estimates from fluctuating weather echoes. The signature is then convolved with the same 5-point radial Gaussian filter used in the signal processor, which reduces the output RMS noise level by a factor of 0.6.

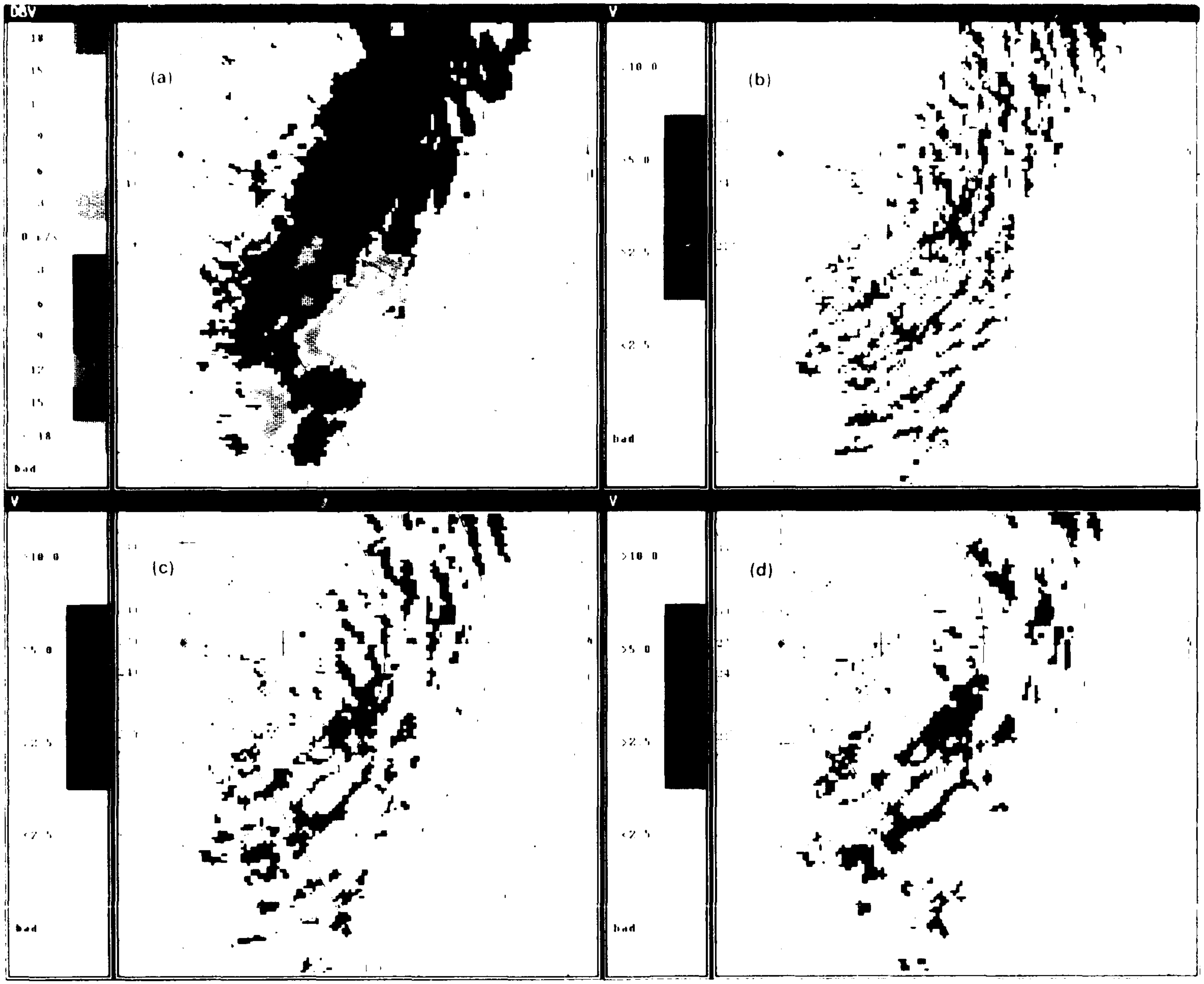

Plate 2.1 (a) The velocity field for one scan through a microburst at the ASR testbed at Huntsville, Alabama on August 15, 1985. (b)-(d) Divergence fields resulting from the application of the least squares estimator with widths of (b) 3 gates (360 m), (c) 7 gates (840 m) and (d) 11 gates (1320 m).

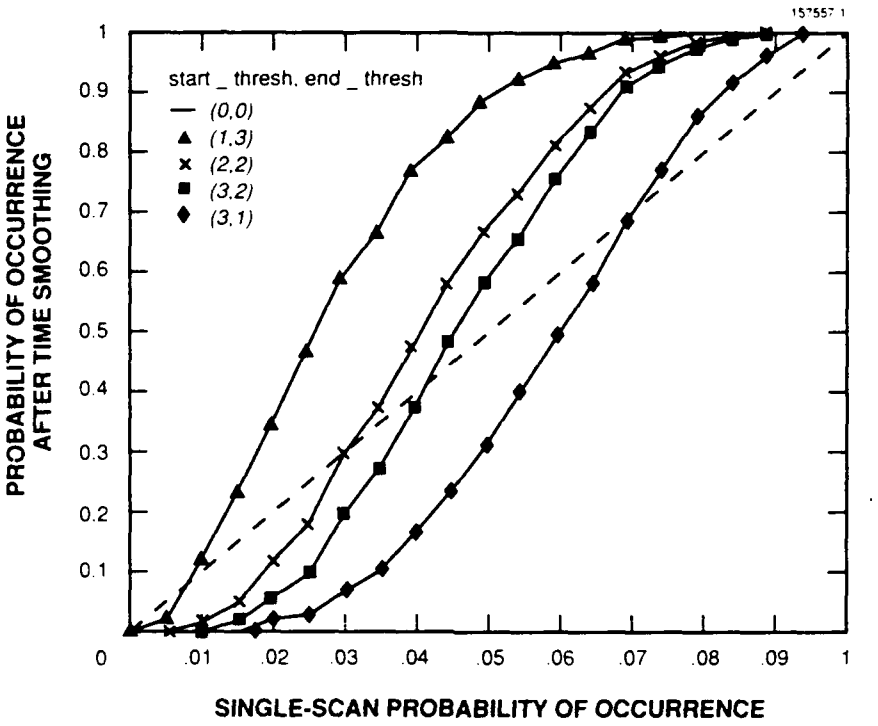

Figure 2.2: Effects of DBA time logic on frequency of features.

The resulting signatures are characteristic of and have noise properties similar to those generated by the ASR signal processor. Figure 2.3 shows a representative set of simulated radial divergence signatures. The strength of the divergence being modeled is 20 m/s, extending over 2 km. The graphs show signature realizations for pre-smoothed velocity estimate RMS errors ranging from 0 to 3 m/s. A variety of actual radial divergence signatures are plotted in Figure 2.4 for comparison. (Note that the spatial scales for the actual signatures differ, and that a higher resolution may cause them to appear more noisy when contrasted to the simulated cases.)

Parameters of amplitude (corresponding to the strength of the divergence), period (corresponding to its radial extent), and velocity estimate RMS error prior to smoothing are varied in the performance analysis. 1500 trials are performed for each control group to provide statistically reliable results.

The study measured both detection performance and false alarm performance. Algorithm detection performance for a single scan was quantified using the percentage of radial overlap of the estimated divergence with that portion of the sine wave exhibiting divergence exceeding 2.5 x 10-3 m/s / m. At this threshold, divergence is considered operationally hazardous to aircraft.

Note: The signal processing operation, which includes not only Gaussian smoothing but also spatial median filtering, is discussed in [Weber, 1989].

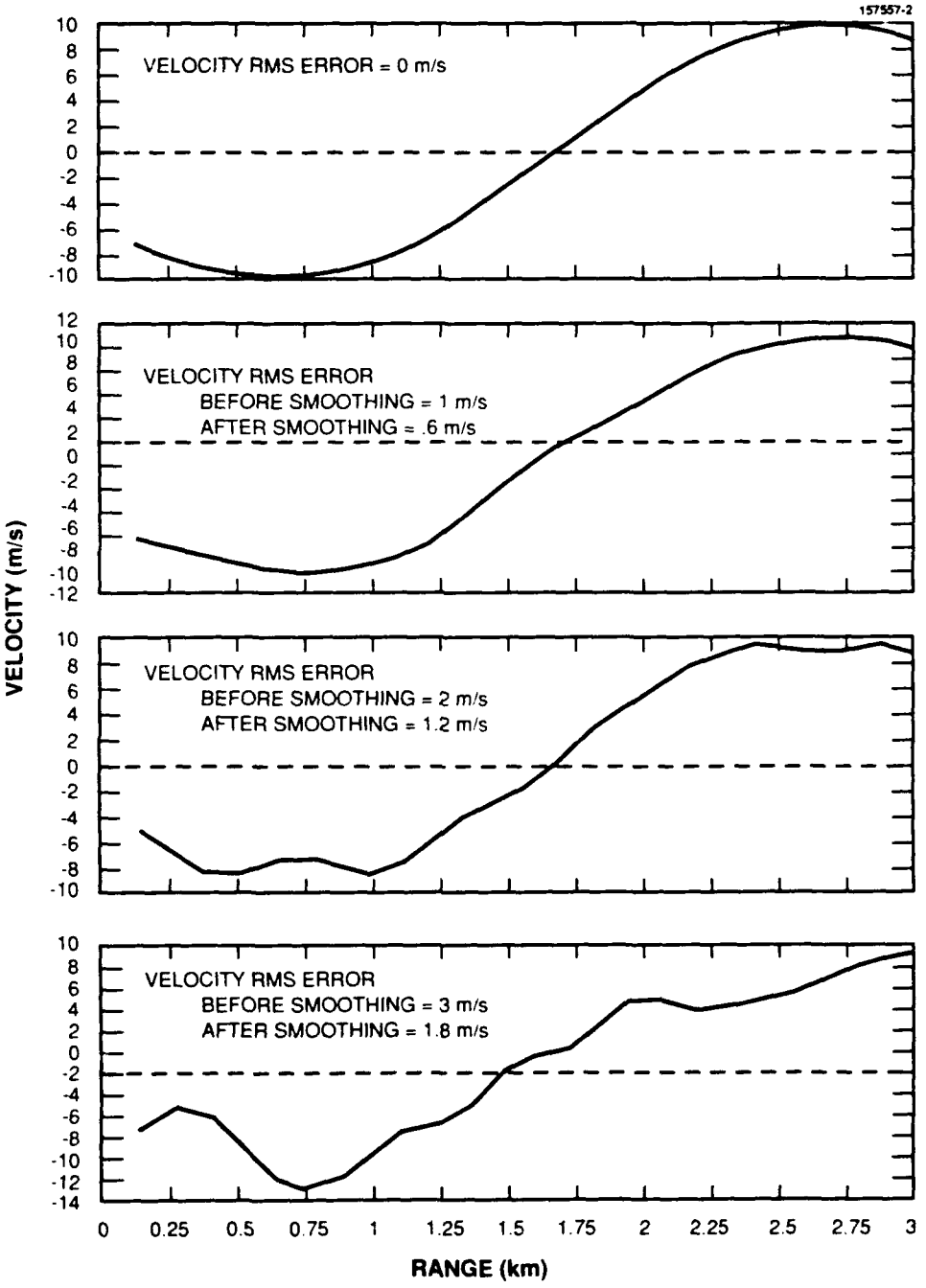

Figure 2.3: Simulated ASR radial divergence signatures.

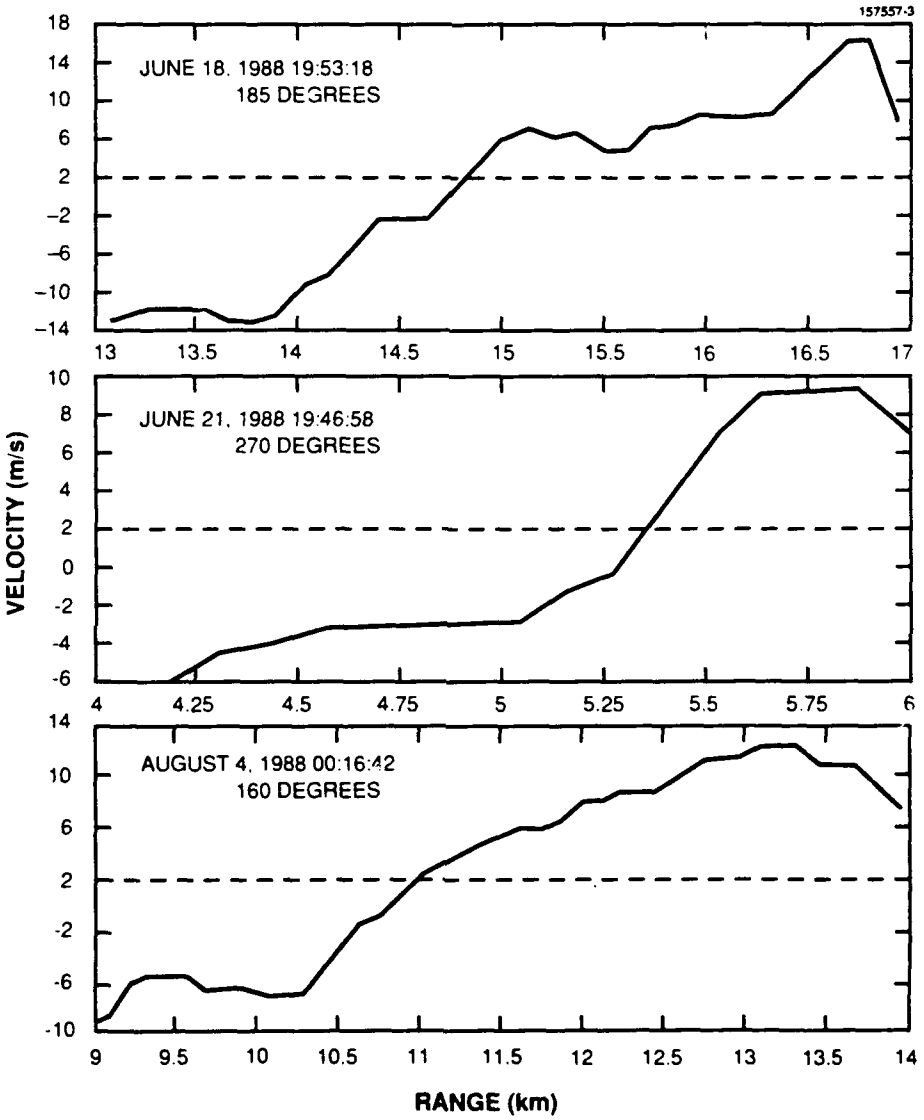

Figure 2.4: Actual radial divergence signatures from experimental ASR.

False alarm immunity was assessed by applying the algorithms to a constant wind profile with added Gaussian velocity errors. The probability of false alarm was computed as the number of algorithm point shear declarations over the total number of points. In the discussion of false alarm immunity, we further reference the graph of Figure 2.2 to show how time smoothing may greatly reduce the false alarm probability of the least-squares technique.

2. Performance Results

Figure 2.5 shows the relationship between percentage of length detected and velocity standard deviation for the divergence-based algorithm using least-squares filter widths ranging from 360 to 1320 m. For comparison, corresponding results from the radial divergence detection phase of the MDOA are also shown. The distance of the hazard signature was fixed at 4 km and the strength at 10 m/s, simulating a microburst of minimum severity. The velocity estimate RMS error prior to Gaussian smoothing was varied from 0 to 3 m/s.

For all methods, the percentage of hazard length detected decreases with increase in the velocity estimate error. For velocity errors less than roughly 1 m/s, the MDOA results in a higher percentage detection than the least-squares filters shown, with the converse applying at larger velocity errors. Coherent integration periods for TDWR have been set so that the velocity estimate standard deviation is less than 1 m/s. For the ASR, however, estimate errors may sometimes be as large as 2 to 3 m/s, even after spatial filtering [Weber, 1989]. Thus, the divergence-based approach may be a more suitable match to the characteristics of velocity fields estimated from ASR signals.

Figure 2.6 shows the percentage of length detected plotted against signature strength. The velocity error was fixed at 3 m/s. For all methods, the percentage of hazard length detected increases with increasing event strength, as we would expect. The MDOA falls short of the least-squares estimators in percentage length detected, again due to the high assumed velocity estimate error.

Figures 2.5 and 2.6 show that the performance of the divergence-based method increases with the length of the window used for the least-squares slope estimate. We know, however, that for a given signature (length, strength and RMS error combination) there exists a filter size at which performance breaks down. To determine a reasonable least-squares filter size to use in all cases, we need to find performance boundaries. One such boundary was found by creating a signature corresponding to a microburst of minimum plausible size, 1 km, and again examining the relationship between algorithm performance and signature strength, shown in Figure 2.7. Again, velocity estimate error prior to smoothing was fixed at 3 m/s. Performance increases with increase in filter size up to 840 m; performance drops by more than 10 percent at the 1080 m filter, and continues to drop with increasing size as the window becomes too large in relation to the signature extent.

The results of Figure 2.7 indicate that a 840 m width window for the least squares fit is the best choice filter size for smaller signatures. Figures 2.5 and 2.6 confirm that its performance is good for larger microbursts.

We will now show that the 840 m window produces acceptable false alarm performance by examining its noise-response when applied to a flat curve with added Gaussian noise. The relationship between probability of false alarm, defined earlier, and velocity estimate error is plotted in Figure 2.8. The MDOA exhibits less sensitivity to noise than the

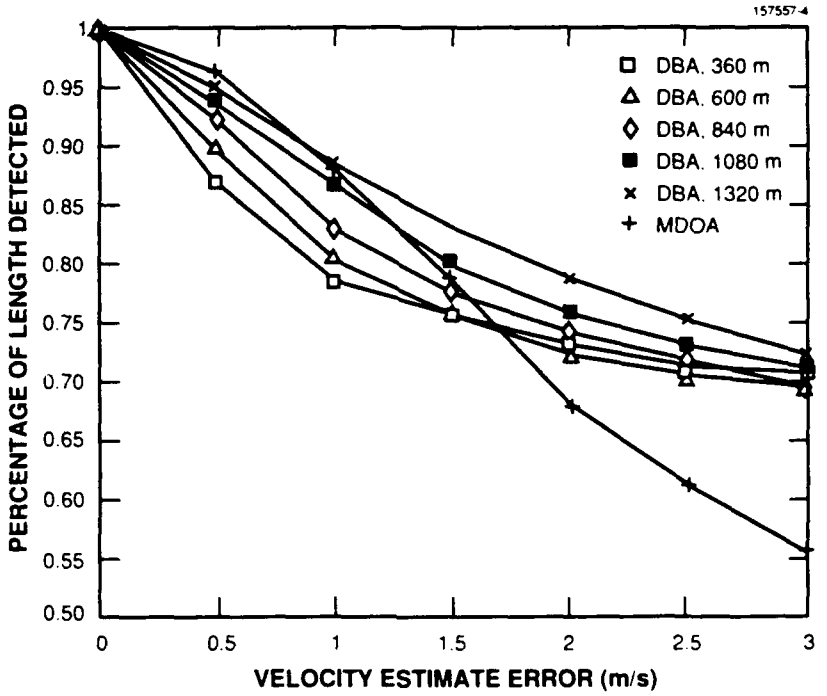

Figure 2.5: Percentage of length detected vs. velocity standard deviation for 4 km event.

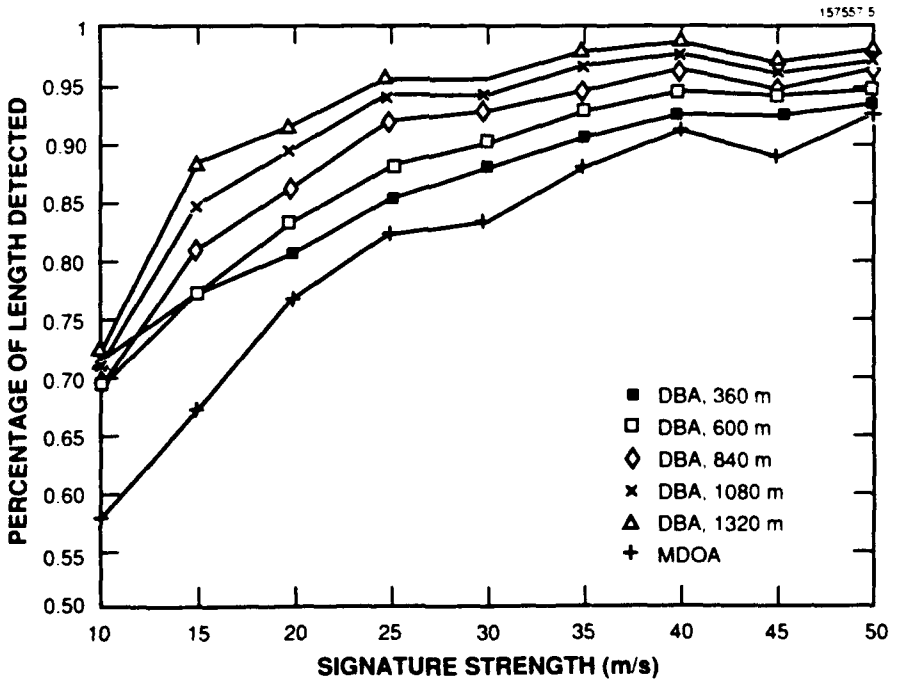

Figure 2.6: Percentage of length detected vs. signature strength for 4 km event.

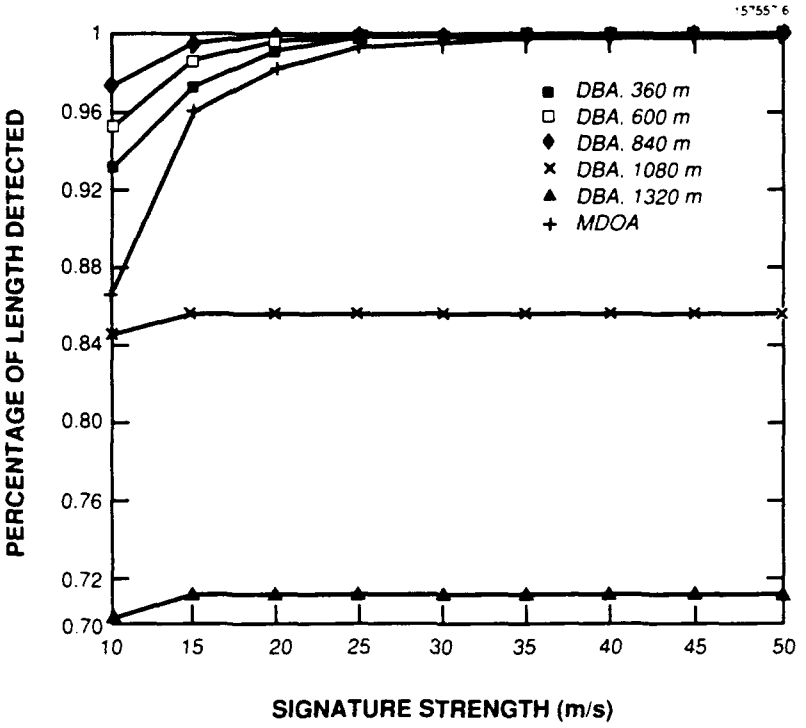

Figure 2.7: Percentage of length detected vs. signature strength for 1 km event.

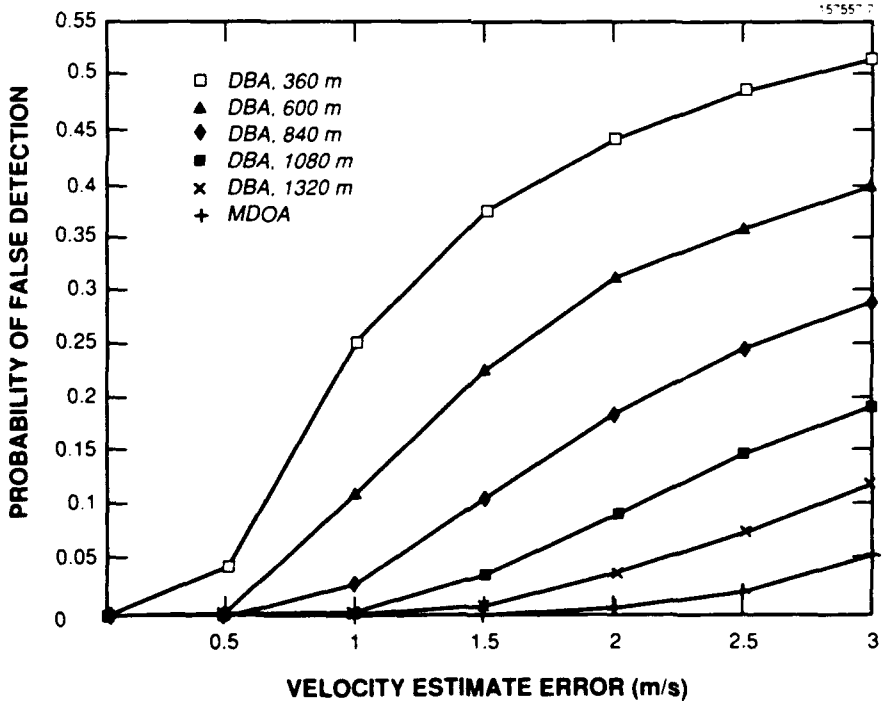

Figure 2.8: Percentage of false alarm vs. velocity standard deviation.

840 m filter and the other least-squares filters at this algorithm stage. This is largely due to the MDOA requirement that the radial signature length exceed .96 km; a signature of this magnitude is unlikely to be noise-induced.

Time continuity requirements combined with connectivity requirements applied at the next stage of the least-squares algorithm achieve a similar low probability of false alarm for the DBA. A "sufficiently low" pointwise probability of false alarm for the least-squares technique is .3, the worst case shown for the 840 m filter size. Referring again to Figure 2.2 we see that a pointwise probability of false alarm of $p = .3$ maps to a .2 probability after time continuity has been imposed. Now consider a 4-neighborhood in our shear field where each pixel is "connected" in an 8-connected sense to every other. If we make the simplifying assumption that the probability a given point shear is false is independent of that of any other, then the probability $P(r)$ that exactly r pixels out of the 4 are false is given by the following formula:

$$P(r) = \binom{4}{r} p^{r} (1-p)^{4-r}$$

Using the above formula with $p = .2$, the following probabilities for the 4-neighborhood hold:

$$P(0)= .4096, \quad P(1)= .4096, \quad P(2)= .1536, \quad P(3)=.0256, \quad P(4)= .0016$$

The probability that 2 or fewer elements of the 4-neighborhood will be falsely detected is greater than 97 percent, and the probability of 1 or none is greater than 80 percent. Thus, it is extremely unlikely that connectivity requirements used in the region formation process will produce a sizeable region out of the false registrations. The 840 m fit window should therefore yield a low probability of false region declaration.

The simulation results contained in this section indicate that a least-squares divergence estimator of appropriate width may perform as well or better than the pattern-based radial shear finding method employed by the MDOA at delineating radial divergence signatures in ASR data. The following section discusses the remaining steps of the DBA: 2-D shear region identification and verification, temporal filtering of shear regions, and shape simplification.

III. DIVERGENCE-BASED MICROBURST DETECTION ALGORITHM

The previous section described the DBA's initial radial divergence estimation process and the subsequent time smoothing of point shear estimates. This section describes the remaining stages of the DBA, which are essential to accomplish a complete detection capability. These include 1) 2-D shear region identification; 2) shear region verification; 3) temporal filtering of shear regions; and 4) shape simplification to derive a final output product.

A. 2-D Shear Region Identification and Verification

The first two stages of the DBA produce a field of values indicating the number of scans over which each cell has exhibited sufficient divergence. Proximate resolution cells exhibiting temporally stable strong divergence -- that is, locations with values exceeding *PT_START_THRESH* -- are grouped to form shear regions using an 8-connected region-based segmentation algorithm. (Eight-connectedness says that each pixel is connected to all its 8 neighbors, so that regions are grown diagonally as well as along radials and across azimuths.)

The segmentation is in essence a directed boundary walk. The boundary list contains pixels which surround a shear region, which are not region elements themselves. The basic philosophy is to "walk" around the shear elements, keeping "non-shear" pixels to the left, to mark off the hazard region.

The segmentation algorithm scans the image in increasing azimuth and increasing range until a shear pixel is found. We are now on the edge of a region, and are initially oriented towards decreasing azimuth as shown in 3.1 (a). The boundary walk is carried out using motions which are combinations of movement and rotation. The following motion sequences are used: 1) move-rotate; 2) rotate-move; or 3) move, to the neighbors shown in 3.1 (b). Rotation and translation cause the base coordinate system to be rotated and translated. 3.1 (c) shows the action-causing patterns used to trace the boundary of a region.

The algorithm applies the following rules, which uniquely determine the set of 8-connected regions for any possible set of image values:

1. If *Pattern 1*, Rotate Clockwise and Store Pixel on Left ($N_{-1,0}$)
2. If *Pattern 2*, Move to $N_{-1,0}$ and Store Pixel on Left ($N_{-1,-1}$)
3. If *Pattern 3*, Move to $N_{-1,-1}$ and Rotate Counterclockwise

Note that a region may be sparse, as long as its outermost pixels are 8-connected.

The boundary walk for a given region ends up where it started. The algorithm continues the search for the next shear region from the first encountered pixel of the last region, skipping sections of the image which have already been traversed.

This technique accomplishes the dual goals of 1) grouping homogeneous elements (adjacent shear pixels) into regions and 2) filling in internal holes by ignoring non-boundary enclosed pixels. Conventional multi-pass raster scan techniques combined with simple post-processing logic could be used to provide the same results. The "walk" method was

used instead because of the small amount of storage required to carry out the segmentation; however, the extra swapping required to traverse the image in a non-raster fashion may cause slowdowns.

For a survey of alternative 8-connected region-based image segmentation methods, see [Rosenfeld and Kak, 1976].

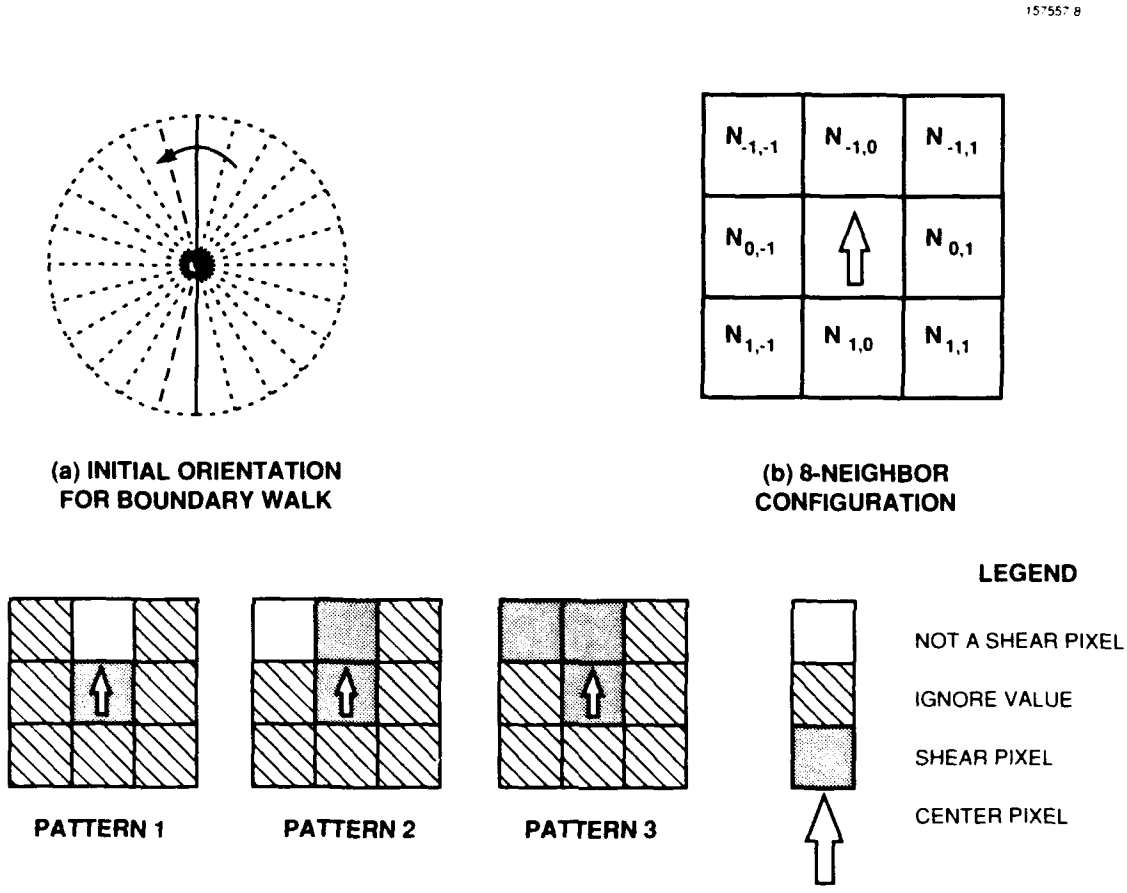

Figure 3.1: Region growing method employed by the DBA.

Would-be regions are filtered using a fixed microburst area threshold. Regions smaller than a user-specified size (*RG_SIZE_THRESH*) are eliminated. The size parameter is meant to reduce anomalies and retain true microburst regions. Other shape properties (such as eccentricity) could be computed in the region growing process to be used for later fast filtering.

A windspeed loss threshold *LOSS_THRESH* is applied to each region. Currently, the loss across a region is computed to be the maximum of the velocity difference across any radial cutting through the region. The threshold is user-specified but is intended to be a lower bound on the windspeed loss that is considered hazardous to aircraft, generally 10 or 15 m/s.

Like the thresholding of point shear estimates, loss thresholding on regions helps to eliminate weak (non-hazardous) divergences. Note that regions surpassing this phase of the algorithm both exhibit a substantial loss *and* are comprised of points which meet a minimum shear criterion.

B. Temporal Filtering of Shear Regions

Logic identical to that used to insure point shear continuity is used to stabilize alarms generated by the algorithm. Without any such logic, borderline regions falling above and below the fixed size and strength thresholds would cause the algorithm to generate inconsistent, intermittent alarms.

The *RG_START_THRESH* parameter specifies the age of a region required for it to be issued as a microburst alarm. A region is determined to match the oldest region on the previous scan which it overlaps. A region which is missing is carried over, or "coasted," until it is missing for *RG_END_THRESH* consecutive scans, at which point it is eliminated.

Figures 3.2 and 3.3 show four consecutive scans collected at the Kansas City FL-3 testbed on May 15, 1989. Figure 3.2 shows the output from the DBA algorithm applied without inclusion of temporal continuity logic. Figure 3.3 then shows DBA output using time parameters *PT_START_THRESH*, *PT_END_THRESH*, *RG_START_THRESH*, and *RG_END_THRESH* set to the values indicated in Section D. The fluctuation in the number and spatial extent of the alarms evident in 3.2 was eliminated by the time correlation logic employed by the algorithm to generate the output of 3.3. In particular, Figure 3.2 exhibits the following:

1. There are six alarms within 15 km in panel a) of Figure 3.2, six in panel b), six in panel c) and five in panel d).
2. The alarms in the southeast quadrant, while of significant size (greater than 2 km^2), exhibit little temporal continuity. Three distinct regions of shear are evident in the four scans, while a maximum of two and a minimum of 1 are detected on any one scan.
3. The alarms to the west and southwest of the radar, in the sweep from 195 to 300 degrees, are fairly consistent.

In Figure 3.3, the sporadic alarms of Figure 3.2 were eliminated, leaving three temporally and spatially consistent alarms to the west and southwest.

C. Shape Simplification

The border of the hazard region is an arbitrary polygon, often with a complicated shape. To simplify interpretation the minimum bounding convex polygon (two dimensional convex hull) of the hazard region is computed as the final output product. The following steps are used to generate the convex hull:

1. Find a point on the convex hull (in our case the first point in the boundary list). Make this the *seed* point, and add it to the list of hull points.
2. Select a *candidate* point. For simplicity, we choose the point following the *seed* point in the boundary list.

3. Compute the equation of the line between the *seed* point and *candidate* point.
4. Determine if all successive boundary points fall to one side of the line. If yes, make the *candidate* the new *seed*, add it to the list of hull points, and go to 2. If no, select a new *candidate* (the point following the current *candidate*) and go to 3.

Figure 3.4 shows a shear region found by the DBA overlaid on a radial velocity field estimated by our experimental ASR. The black outline shows the region of strong divergence and the simpler red shape its associated convex hull. The outlines bound the area where an airplane would experience significant headwind loss (insofar as the hazard region can be determined from single-doppler data.)

D. Algorithm Parameters

The following definitions are provided for the algorithm parameters, with example settings in brackets.

LSQ_WIN_SIZE [7]: The number of gates (each gate spanning 120 meters) for the least-squares linear fit.

DIV_THRESH [2.5 x 10^{-3} /s]: The value used to threshold the field of least-squares divergence estimates.

PT_END_THRESH [2]: If shear at a location does not exceed DIV_THRESH for PT_END_THRESH consecutive scans, its positive map value is set to 0, eliminating its consideration as a shear region element.

PT_START_THRESH [3]: A threshold on the positive map, or number of scans over which sufficient shear must have been seen at a point for it to become part of a shear region.

RG_SIZE_THRESH [1.0 km^2]: The minimum area required of a shear region.

LOSS_THRESH [10 m/s]: The minimum windspeed loss required across a shear region.

RG_END_THRESH [2]: If an alarm has dropped out for RG_END_THRESH consecutive scans, it is eliminated. Otherwise, it is "coasted."

RG_START_THRESH [2]: The scan age of a region required for it to be issued as a microburst alarm.

The following section presents additional case studies of algorithm performance on real data.

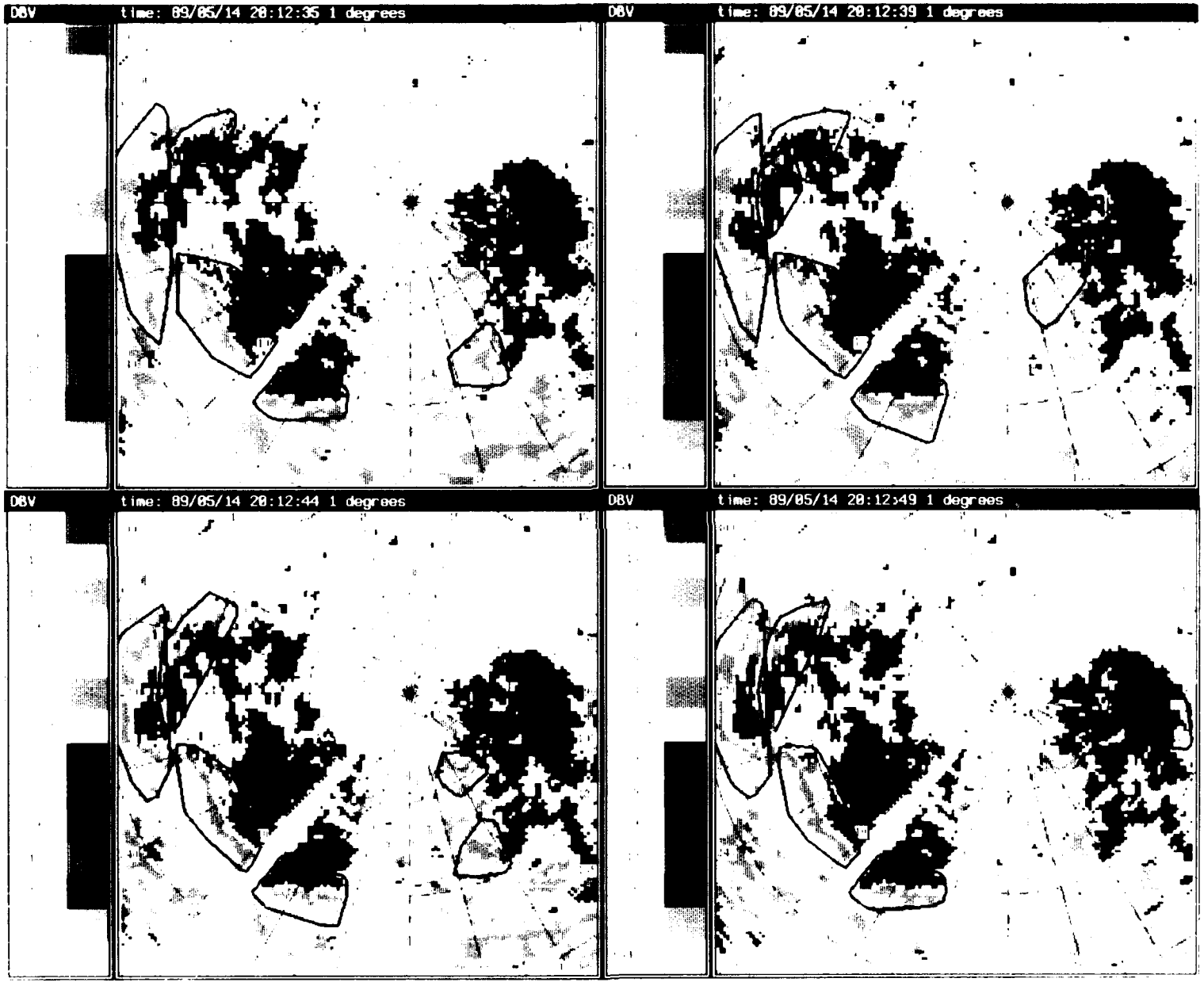

Figure 5.2: Output from DBV applied without temporal continuity logic overlaid on radial velocity field of storm of May 15, 1989.

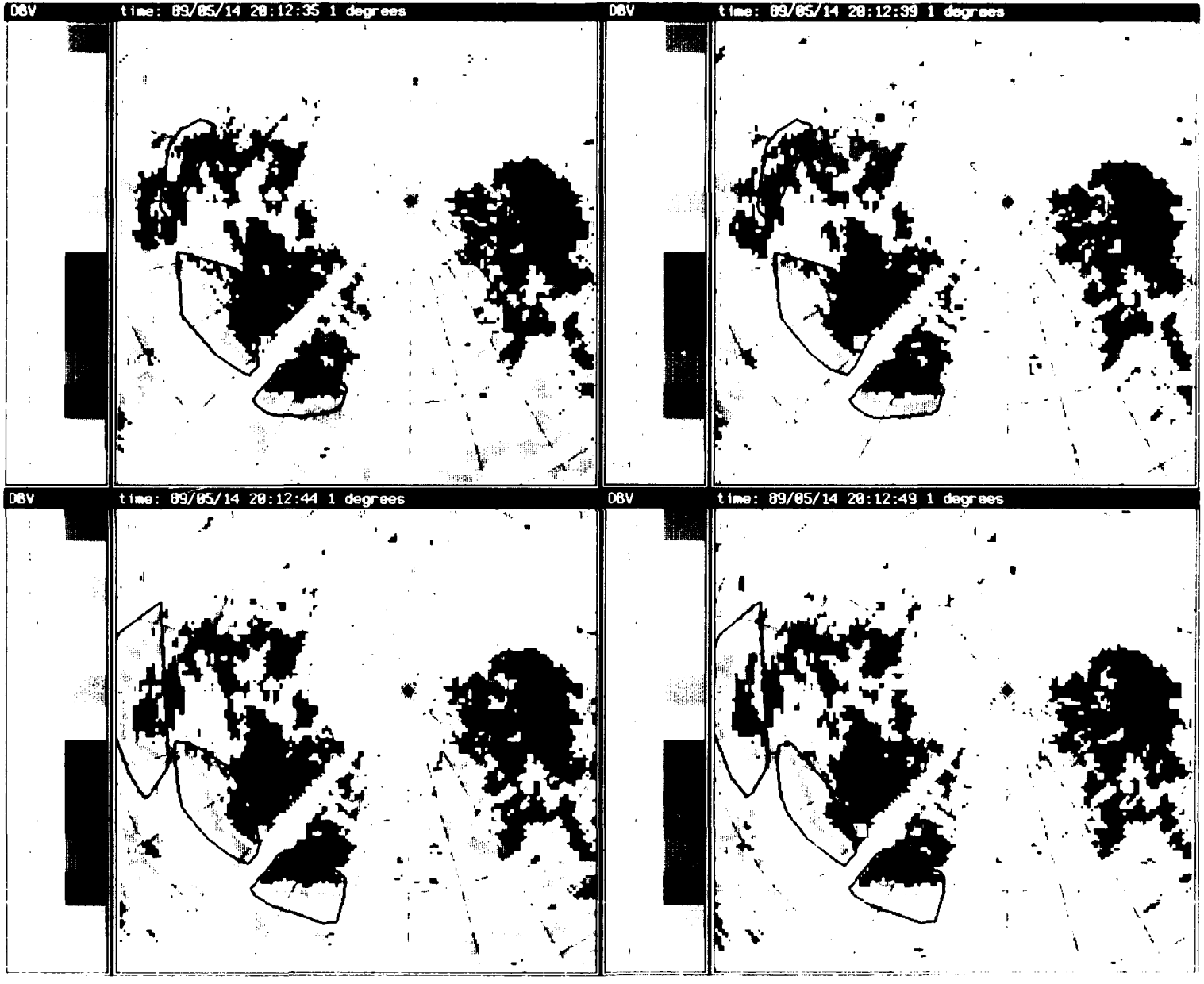
DBV
time: 89/05/14 20:12:35 1 degrees
DBV
time: 89/05/14 20:12:39 1 degrees
DBV
time: 89/05/14 20:12:44 1 degrees
DBV
time: 89/05/14 20:12:49 1 degrees

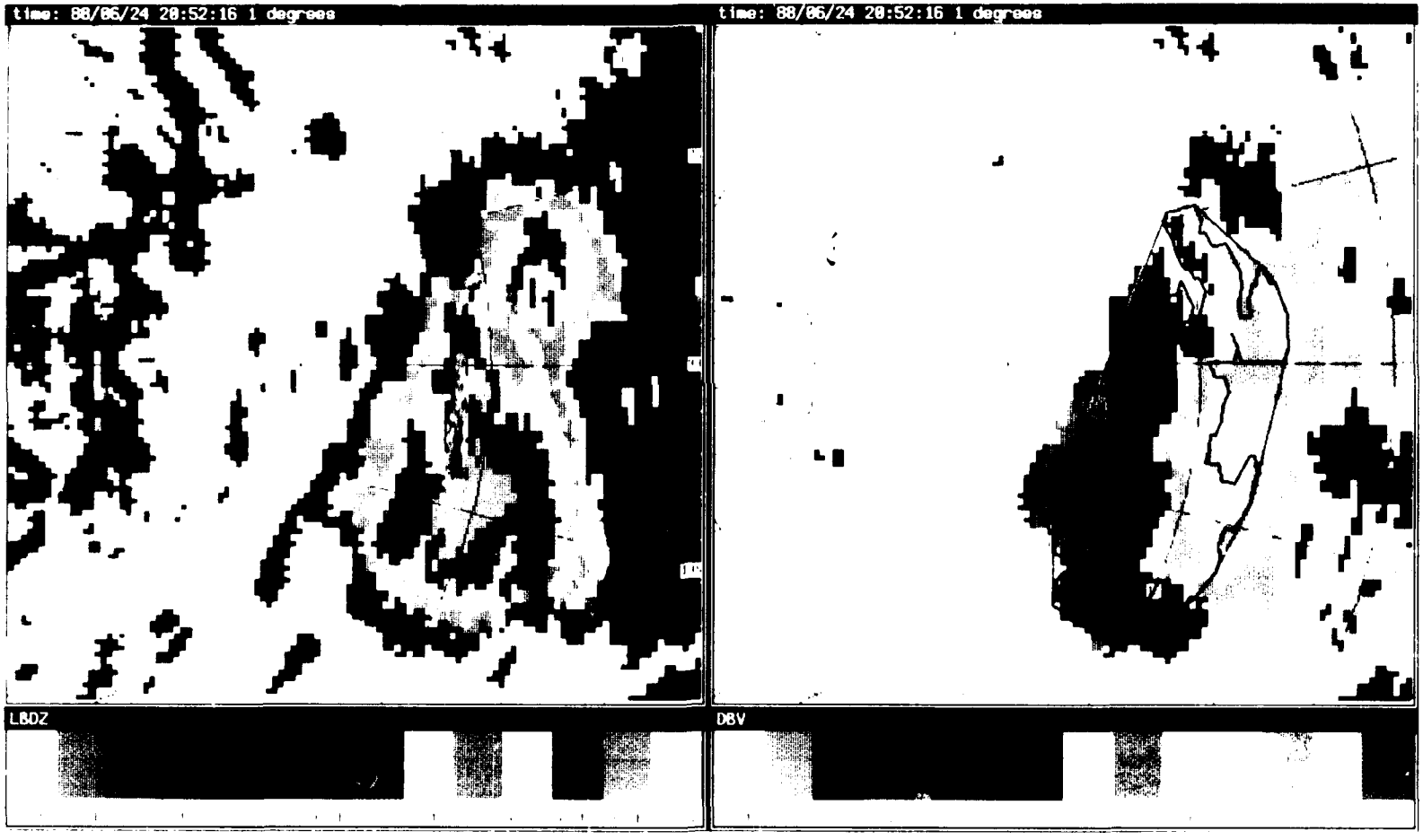
time: 88/06/24 20:52:16 1 degrees
time: 88/06/24 20:52:16 1 degrees
LBDZ
DBV

IV. EMPIRICAL RESULTS

This section presents algorithm results for data collected during our 1988 field experiment in Huntsville, Alabama and during our 1989 experiment in Kansas City, Missouri. A representative set of divergence signatures which occured within 16 km of the ASR have been chosen. Color pictures and algorithm performance statistics have been included.

A. Case Studies

For the cases presented below, final output declarations (hollow geometric shapes) from both the DBA and the ASR Real-Time MDOA algorithms are shown superimposed on the corresponding ASR velocity product.

The output of the ASR DBA is the minimum bounding convex polygon, or convex hull, surrounding the 8-connected elements of a divergence region (refer to Section III, Divergence-Based Microburst Detection Algorithm).

The ASR Real-Time MDOA output is shown as the convex hull for the radial shear segments associated with a microburst alarm. In the current TDWR operational system, the final output is depicted as a bandaid. The bandaid shape fitting algorithm is described in Wilson et. al [1989].

The spatial extent of regions detected by both algorithms in most cases is similar, but not in general coincident. The DBA detects loss regions comprised of point elements containing significant divergence, while the MDOA first detects loss regions comprised of monotonically increasing velocity segments, and then "crops" these segments using shear criteria. Radial and azimuthal extents may differ because of this basic difference in design philosophies between the two algorithms.

MDOA segments currently must meet a minimum radial length requirement of .96 km, while the DBA has no such criterion. In some cases, this causes the DBA alarms to have a larger azimuthal extent.

The two cases below, one from Huntsville in 1988 and the second from Kansas City in 1989, emphasize the similarity in the performance of the two algorithms.

1. 18 June 1988

On June 18, 1988 a divergence region formed 15 km south of the radar at 19:51 GMT. The divergence reached a peak strength of ΔV_R = 32 m/s at approximately 19:55. Figure 4.1 shows 4 scans taken at 30 second intervals around the time of peak shear. The black outlines correspond to superimposed DBA output, and white to that of the MDOA.

This case was chosen as a fairly simple first example. The radial extent of the alarms from each of the algorithms is roughly identical. Alarms from the DBA are wider azimuthally. Figure 4.2 sheds light on the difference in shape. Panel (a) shows the dual-beam velocity product at 19:53:18 with algorithm outputs overlaid. Again, black outlines represent DBA alarms, and white MDOA alarms. Panel (b) shows the intermediate "positive map" product input to the algorithm's region growing process. The color map of (b) was chosen to display, in red, points at which the algorithm has determined sufficient shear to exist. The DBA shape encloses the long arm of shear which extends south of the more symmetric region above. The MDOA would throw this arm, comprised of only a few gates, away. The DBA treats it as significant because it is connected to the larger region.

2. 23 July 1989 - 00:21 to 00:43

Late afternoon thunderstorms in the Kansas City area produced two long-lived divergences within 20 km of FL-3 during the time period, both reaching a peak strength of 20 m/s. Figure 4.3 shows algorithm alarms superimposed on the dual beam velocity product for 4 scans sampled at roughly 3 minute intervals in the middle of the activity. This case also exhibits the similarity in algorithm performance. For the two divergence signatures observed on the scans shown, the DBA output (depicted in black) and the MDOA output (depicted in white) are roughly coincident. Note that the microburst to the south of the radar (180 degrees, 6 km) was detected by the DBA slightly earlier.

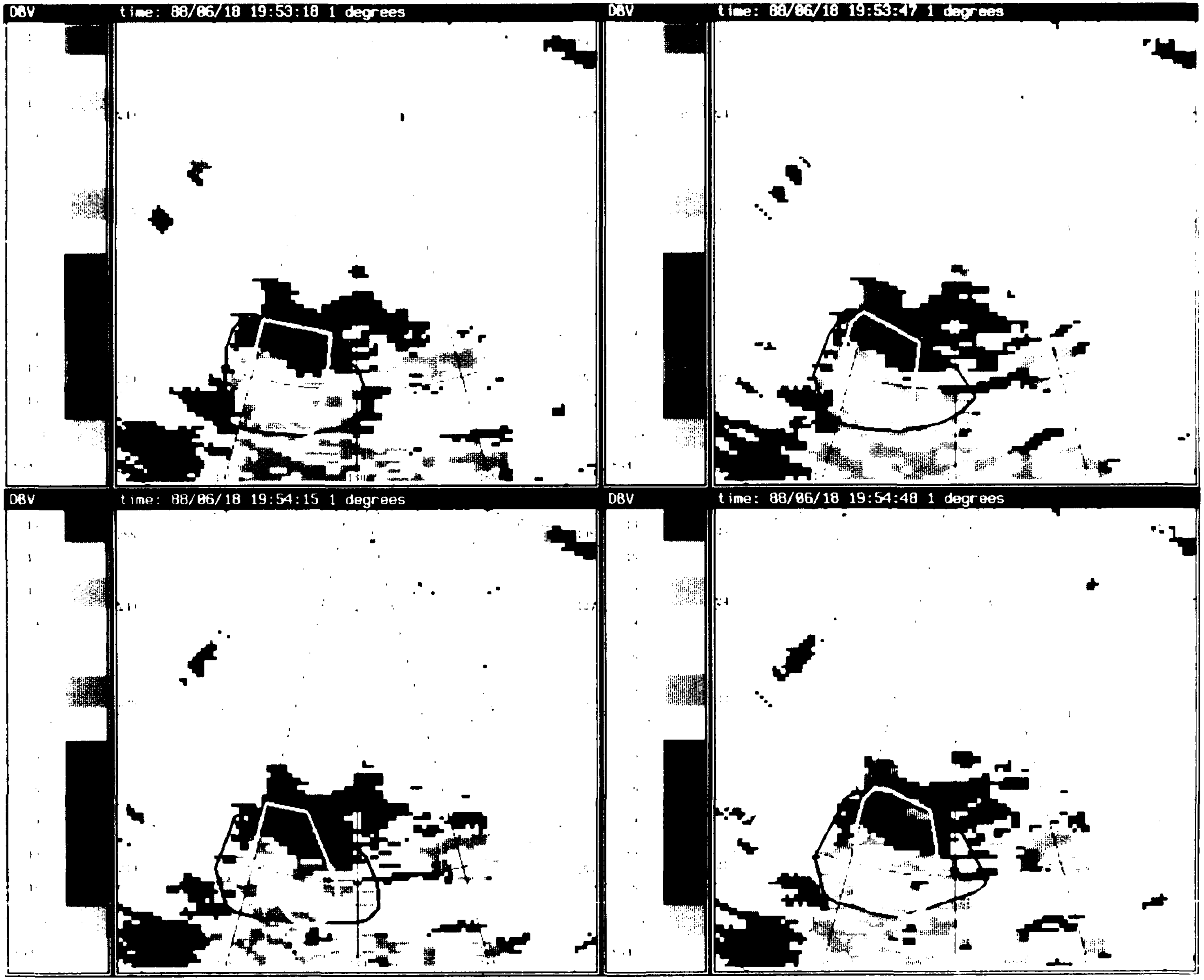

[illegible] 4.1. Radial [illegible] field for sequence of scans through microburst [illegible] June 18, 198[illegible] [illegible]
[illegible] and [illegible] and MDOA [illegible] in white

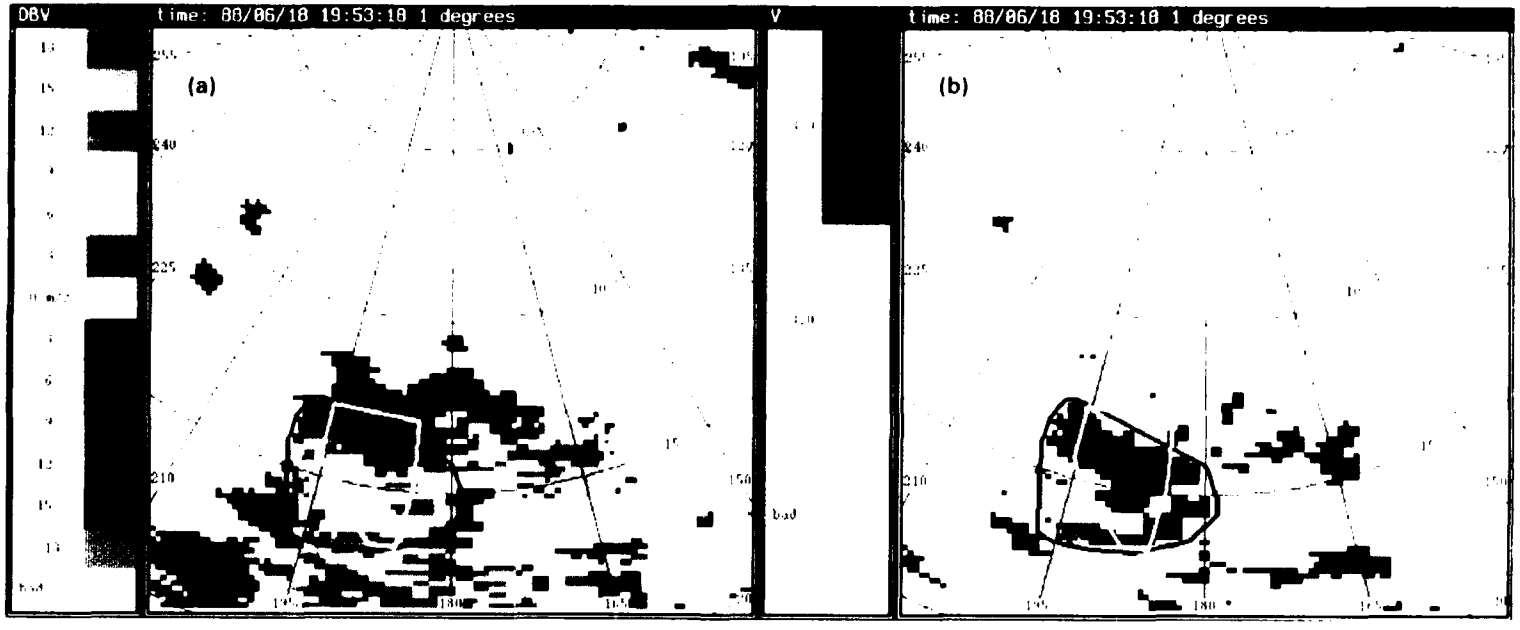

Figure 4.2: Microburst of Figure 4.1 at 19:53:18. (a) dual-beam velocity. (b) intermediate positive map product. Time-continuous shear pixels are displayed in red. (a) and (b) DBA alarms are overlaid in black and MDOA alarms in white.

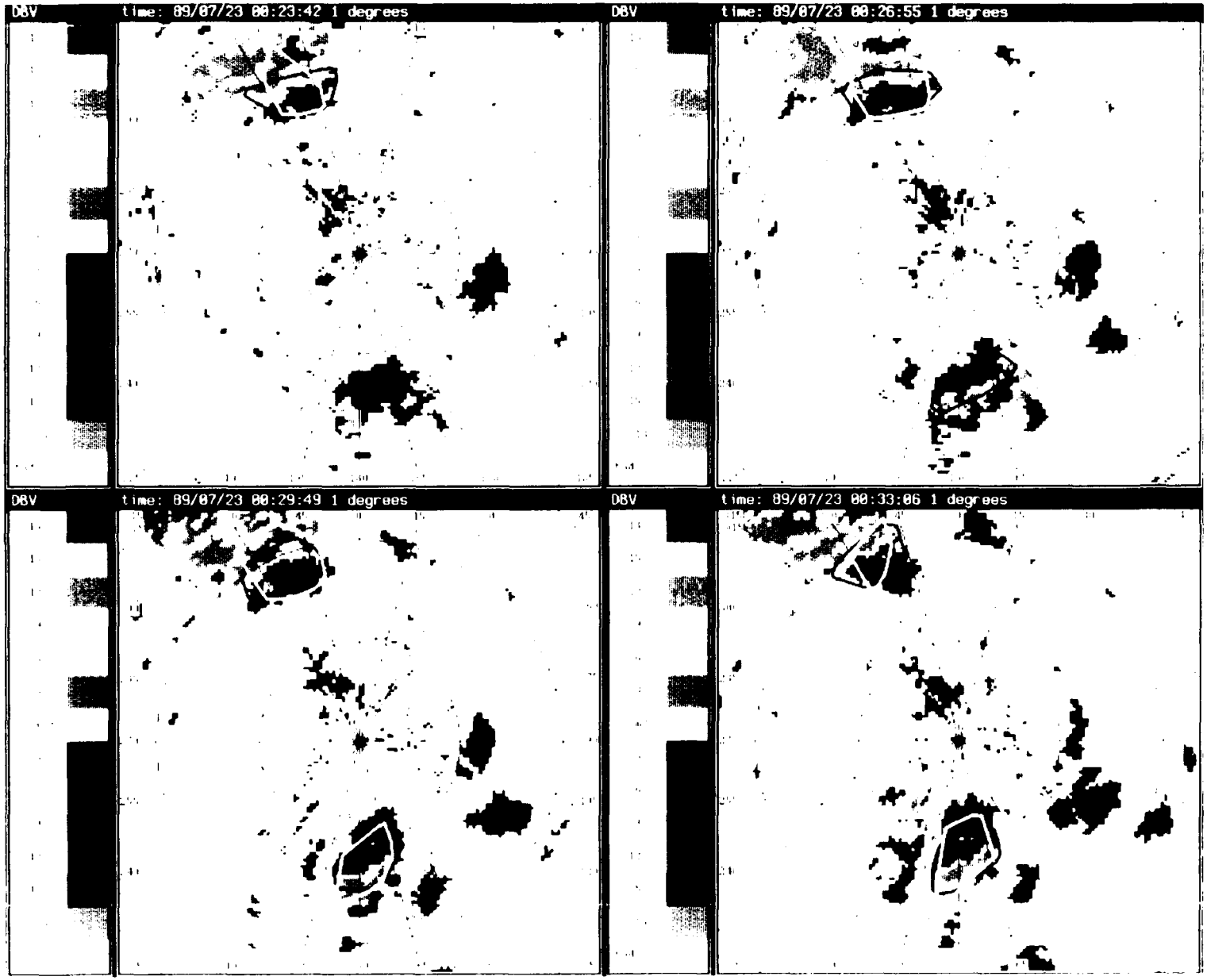

Figure 4.3 Radar echo [illegible] sequence of scans through microburst [illegible] July 23, 1989. DBV scale [illegible] Radar at MIT Lincoln Laboratory.

B. Automated Scoring

1. Scoring Methodology

Reflectivity and velocity images from the ASR were examined by a trained meteorologist to determine the existence of a divergence signature, its strength, and its spatial extent. These polygonal "truth" events were entered into a computer database for access by an automated scoring process. Because this report focusses solely on algorithm performance assessment and not on radar velocity estimate accuracy the ASR is used for truth instead of the colocated pencil beam radar used in earlier studies [Weber and Noyes, 1988]. Thus, missed detections or false alarms caused by errors in velocity field estimates are not reflected in these statistics.

The automated scoring process reads the truth database and algorithm archive database to compute the overlap between truth and algorithm output. The specific scoring rules used are as follows:

1. If the area of a truth event is overlapped by the union of algorithm alarms, that truth event is considered a *hit*.
2. If the area of an algorithm alarm is *not* overlapped by the union of truth events, that alarm is considered *false*.

Note that this scoring methodology is more stringent than that used in [Weber and Noyes, 1988, 1989] which was based on previous procedures employed by the TDWR groups at Lincoln Laboratory and the National Center for Atmospheric Research (NCAR). These had merely required 2 km proximity, and allowed for "early" or "late" algorithm alarms.

The performance metrics tabulated below are:

Detection Probability (POD) - the number of detected divergence signatures divided by the total number of divergence signatures

False Alarm Probability (PFA) - the number of algorithm alarms not associated with valid divergence signatures divided by the total number of alarms

2. Scoring Results

The table below presents detection statistics for divergence signatures centered within a 16 km range of the ASR. 4 days from Huntsville, Alabama in 1988 and 2 days from Kansas City, Missouri in 1989 are included, encompassing a total of more than 1000 scans, 100 minutes and 25 events. The following time periods are included in the scoring statistics:

1. 18 June 1988 - 19:51 to 20:02
2. 21 June 1988 - 19:46 to 20:14

3. 24 June 1988 - 21:18 to 21:27
4. 4 August 1988 - 00:15 to 00:27
5. 24 June 1989 - 20:55 to 21:14
6. 23 July 1989 - 00:21 to 00:43

The following statistics should be viewed as rough estimates of algorithm performance. The subjectiveness and impreciseness of meteorological truth is likely to cause small quantitative errors in the calculation of statistics. Attributes of area and severity which are subjected to strict minimum requirements by the algorithms are not measured precisely with the human eye. In addition, shears embedded in the environmental flow which do not exhibit a clearly visible negative-positive velocity couplet may be missed by the human expert. While these embedded shear phenomena may be microburst hazards, they may also be artifacts caused by a vertically sheared environment.

Table 4.1: Divergence Signature Detection Performance as a Function of Outflow Strength

		ΔV_R > 15 m/s	ΔV_R > 20 m/s	ΔV_R > 25 m/s
Divergence-Based Algorithm	POD	.98	.99	1.00
	PFA	.08	.06	.01
ASR Real-Time Microburst Divergent Outflow Algorithm	POD	.98	1.00	.99
	PFA	.08	.03	.01

The two algorithms exhibit roughly equivalent detection performance overall, with minor differences on individual cases. The slightly higher occurrence of DBA false alarms results from the DBA's detection of a long-lived radar-generated false alarm on June 24, 1989.

V. SUMMARY

This report has described and evaluated a divergence-based microburst detection algorithm developed for the ASR. This technique was developed as a research tool to investigate alternatives to the TDWR microburst algorithm initially adopted for the ASR. Roughly equivalent performance was derived from application of the two techniques to data collected during isolated air mass thunderstorms at our testbeds in Huntsville, Alabama and Kansas City, Missouri.

The following discussion highlights the significant differences in approach between the two algorithms, referring to the analysis contained in previous sections to analyze their effectiveness.

The first stage of the DBA computes radial divergence at a point by performing a least squares linear fit to the elements in the surrounding radial window. Section II showed that such an approach does indeed contain performance tradeoffs in noise resiliency versus spatial accuracy. A too-small window may accurately respond to true signals but improperly key on isolated noise points, and a too-large window may reduce the effects of velocity noise, but spatially under- or overestimate the hazard extent. We were able to show that a fixed least-squares window size can be found which exhibits reasonable performance over the entire range of radial divergence signatures expected for real microbursts.

The DBA's linear least-squares fit approach to computing pointwise radial divergence has a closed-form mathematical representation. The one variable which can effect the outcome of the process on a given data set is the size of the estimation window. In contrast, the segment growing process of the MDOA is a nonlinear multi-decision-based process, making an analytic description of its behavior difficult. We view the simplicity of the low-level shear finding portion of the DBA as a great strength.

The DBA applies time continuity constraints to individual point shear elements. This approach takes advantage of the ASR's rapid rotation rate of 4.8 seconds, and was the basis for the logic described by Newell [1990] which time smooths the segments found by the ASR Real-Time MDOA.

The DBA groups elements of the "time indicator" field output by the first two stages of the algorithm into two-dimensional 8-connected shear regions. The MDOA algorithms, on the other hand, first grow one-dimensional radial regions, or segments, and then associates these azimuthally. The DBA approach finds divergence estimates and grows regions in two separate stages. The MDOA algorithms identify divergence points and grow radial segments simultaneously, making it more difficult to evaluate each process. The interdependency of algorithm stages makes the empirical determination of an optimal parameter set for the MDOA difficult.

Based on the above observations, we can make the following statements:

1. analysis to date indicates cumulative performance is the same for both methods on the cases evaluated thus far.

2. the DBA approach shows *strength-in-simplicity*. It steps are very compartmentalized, and the shear finding computation has a simple mathematical representation. By contrast, the MDOA's shear finding process is interwoven with the radial region growing process, and is decision-based and highly nonlinear.

3. the DBA computes shear and requires substantive shear at each point for it to become part of a two-dimensional hazard region. The MDOA algorithms first detect one-dimensional loss regions comprised of monotonically increasing velocity segments, and then "crop" these segments using shear criteria. These segments are then grouped into two-dimensional regions. Both the DBA and MDOA algorithms impose a windspeed loss threshold.

4. simulation analysis indicated that a least squares fit window size exists for which the radial divergence estimation phase of the DBA exhibits acceptable "percentage length detected" performance over all reasonable microburst scales and velocity error assumptions; the same analysis showed that the MDOA performs less well for extreme-noise conditions.

5. simulation analysis indicated that, when applied to a constant radial wind profile with added Gaussian noise, the least-squares operator generates a greater number of false detections at individual range gates than the MDOA algorithm. However, these false detections are reduced considerably by the DBA's subsequent time smoothing and region filtering operations.

6. the DBA takes advantage of the ASR's rapid update rate by applying time continuity constraints to pointwise shear estimates. The ASR implementation of the MDOA applies similar logic to shear segments.

The processing requirements of the divergence-based algorithm exceed those of the ASR real-time MDOA. The DBA takes on average 10 seconds and a maximum of 30 seconds to process a single scan on a Sun 3/80 Workstation. The MDOA matches the 4.8 second scan rate of the ASR when run on the Mizar 68030 single-board computer, a CPU with roughly equivalent performance as the Sun 3/80. To adapt the DBA for real-time, we have two alternatives: 1) re-implement the DBA, concentrating on code optimization and "shortcuts"; and 2) run the DBA on a faster architecture.

The DBA will be implemented in real-time and will serve as the basis for an ASR wind shear processor specification if continued analysis is favorable.

APPENDIX A: BRIEF OVERVIEW OF THE REAL-TIME ASR MICROBURST DIVERGENT OUTFLOW ALGORITHM

Sections II and IV of this report use the Microburst Divergent Outflow Algorithm (MDOA) as a yardstick to evaluate the performance of the divergence-based algorithm (DBA). The simulation study of Section II employs a version of the MDOA adapted from TDWR in 1987.* A further adaptation for real-time ASR use, which generated the results in Section IV of this report, was made by Newell [1990]. The segment detection phase of that algorithm is described below.

The first phase of the ASR Real-Time MDOA slides out along a radial to search for a sequence of monotonically increasing velocities, or a "segment", like that shown in A.1. The segment search and validation are comprised of several phases:

- BEGIN SEGMENT
  1. Search for a velocity increase on two adjacent gates which is smaller than *MAX_FIRST_INCREASE* (5.0 m/s). This is the segment start.

     As the algorithm proceeds from gate to gate along the segment, a variable called *sum_decreases* is used to keep track of the sum of gate to gate velocity decreases.

  2. At the beginning of each segment, initialize the value of *sum_decreases* to *INIT_SUM_DECREASES* (-2.0 m/s). This has the effect of reducing the tolerance for decreasing trends that occur early in the segment.
- GROW SEGMENT UNTIL TERMINATION CONDITIONS (3 or 4) ARE MET
  3. Terminate the segment if more than *MAX_BAD_VALS* (2) are encountered.
  4. Terminate the segment if the sum of decreases since the most recent maximum value is greater than *MAX_SUM_DECREASES* (-5.0 m/s).

     5 and 6 describe the rules used to modify the value of *sum_decreases*.

  5. When a velocity increase is found, increment the value of *sum_decreases* by *CONSTANT_INCREASE* (1 m/s), or set it to 0.0 when it exceeds 0.0. The reason to increase it by a constant instead of the actual value of the velocity increase is to weigh the decreasing trends more heavily in regions where the velocity field is oscillating up and down. This tends to terminate the growth phase of noisy segments with greater efficiency.
  6. When a velocity decrease is found, the actual value of the decrease is added to *sum_decreases*.

---

* Note that the TDWR MDOA algorithm described in Merritt [1987] has since undergone changes. Results from the revised algorithm are described in Merritt et al. [1989].

- PERFORM SEGMENT VALIDATION:

  7. The length of the segment must be greater than or equal to *MIN_SEG_LENGTH* (.96 km).

  8. Segments must exhibit a differential velocity greater than or equal to *MIN_SEG_DIFF* (8.0 m/s).

  9. The shear slope at each point in the segment must exceed *MIN_SEG_SLOPE* (1.8 m/s / km). The slope at each point is calculated using both an 11-point and a 7-point window (centered at the test point), except near the beginning and end of a segment, where a shorter single window (3, 5, 7 or 9) is used to avoid overlapping the endpoints. If the slope at any point is less than the threshold, the segment is split at that point. Any segment that is split must pass through steps 7, 8 and 9 again.

Later algorithm stages perform segment temporal smoothing, group range-overlapping segments on neighboring radials into candidate hazard regions, and perform spatial and time filtering on those.

The final output of the ASR Real-Time MDOA is a database archive file containing microburst alarms with geometric, strength and time properties.

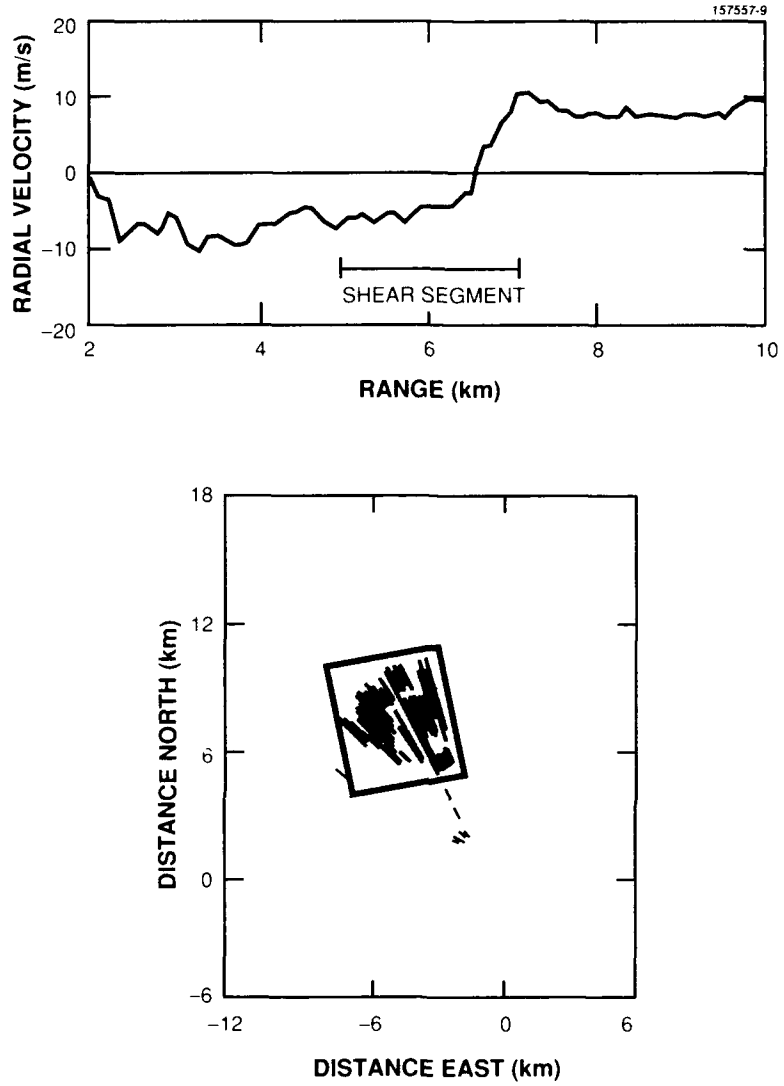

Figure A.1: MDOA Shear Segment Detection and Association (from [Merritt, 1987])

REFERENCES

K.L. Elmore and W.R. Sand, "A Cursory Study of F-Factor Applied to Doppler Radar," *3rd International Conference on the Aviation Weather System*, Anaheim, CA, American Meteorological Society, Boston, MA, 1989.

M.W. Merritt, "Automated Detection of Microburst Windshear for Terminal Doppler Weather Radar," SPIE Vol. 846, *Digital Image Processing and Visual Communications Technologies in Meteorology*, pp. 61-65, 1987.

M.W. Merritt, D. Klingle-Wilson and S.D. Campbell, "Wind Shear Detection with Pencil-Beam Radars," *The Lincoln Laboratory Journal*, Vol. 2, No. 3, pp. 483-510, 1989.

O.J. Newell, Personal Communication, Lincoln Laboratory, MIT, 6/19/90.

A. Rosenfeld and A.C. Kak, A.C., *Digital Picture Processing*, Academic Press, New York, U.S.A., 1976.

M.E. Weber and T.A. Noyes, "Low-Altitude Wind Shear Detection with Airport Surveillance Radars: Evaluation of 1987 Field Measurements," Project Report ATC-159, Lincoln Laboratory, MIT, FAA/PS-88/10, 1988.

M.E. Weber, "Dual-Beam Autocorrelation Based Wind Estimates from Airport Surveillance Radar Signals," Project Report ATC-167, Lincoln Laboratory, MIT, FAA/PS-89/5, 1989.

M.E. Weber and T.A. Noyes, "Low-Altitude Wind Shear Detection with Airport Surveillance Radars," *The Lincoln Laboratory Journal*, Vol. 2, No. 3, pp. 511-526, 1989.

F.W. Wilson, K. Brislawn and R.K. Goodrich, "Divergence Estimation by a Single Doppler Radar," *3rd International Conference on the Aviation Weather System*, Anaheim, CA, American Meteorological Society, Boston, MA, 1989.